TFEB acetylation promotes lysosome biogenesis and ameliorates Alzheimer's disease–relevant phenotypes in mice

Received for publication, December 28, 2021, and in revised form, September 19, 2022 Published, Papers in Press, October 27, 2022,
https://doi.org/10.1016/j.jbc.2022.102649

Tianyou Li[‡], Limin Yin[‡], Xinyi Kang[‡], Wenlong Xue[‡], Ning Wang, Jie Zhang, Ping Yuan, Lingxi Lin, and Yang Li*

From the Department of Pharmacology, State Key Laboratory of Medical Neurobiology and MOE Frontiers Center for Brain Science, Key Laboratory of Metabolism and Molecular Medicine, Ministry of Education, School of Basic Medical Science, Fudan University, Shanghai, China

Edited by Qi-Qun Tang

Lysosomes are one of the major centers for regulating cargo degradation and protein quality control. Transcription factor EB (TFEB)–promoted lysosome biogenesis enhances lysosome-mediated degradation and alleviates neurodegenerative diseases, but the mechanisms underlying TFEB modification and activation are still poorly understood. Here, we report essential roles of TFEB acetylation in TFEB nuclear translocation and lysosome biogenesis, which are independent of TFEB dephosphorylation. By screening small molecules, we find that Trichostatin A (TSA), the pan-inhibitor of histone deacetylases (HDACs), promotes nuclear translocation of TFEB. TSA enhances the staining of cells by LysoTracker Red and increases the expression of lysosomal and autophagic genes. We identify four novel acetylated lysine residues in TFEB, which are important for TFEB nuclear translocation and lysosome biogenesis. We show that TFEB acetylation is regulated by HDACs (HDAC5, HDAC6, and HDAC9) and lysine acetyltransferases (KATs), including ELP3, CREBBP, and HAT1. During TSA-induced cytosol-to-nucleus translocation of TFEB, acetylation is independent of TFEB dephosphorylation, since the mTORC1- or GSK3β-related phosphorylation sites on TFEB are still phosphorylated. Administration of TSA to APP/PS1 mice increases the expression of lysosomal and autophagic genes in mouse brains and also improves memory. Accordingly, the β-amyloid plaque burden is decreased. These results show that the acetylation of TFEB, as a novel mechanism of TFEB activation, promotes lysosome biogenesis and alleviates the pathogenesis of Alzheimer's disease. Our results also suggest that HDAC inhibition can promote lysosome biogenesis, and this may be a potential therapeutic approach for the treatment of neurodegenerative diseases and disorders related to HDAC hyperactivation.

Lysosomes are one of the major degradative organelles that maintain cellular metabolism and homeostasis (1–5). During the pathogenesis of neurodegenerative diseases, such as Alzheimer's disease (AD), accumulation of protein aggregates becomes more and more severe, which is partially due to defective degradation in patients' brains (6–8). Thus, it is important to uncover the regulatory mechanisms of lysosome biogenesis to enhance lysosomal degradation.

Recent studies have shown that lysosome biogenesis is controlled by transcription factor EB (TFEB) and repressor Zinc finger protein with KRAB and SCAN domains 3 (ZKSCAN3) (9–12). Under the condition of starvation, especially the deprivation of amino acids, the activity of mTORC1 is reduced, which subsequently results in dephosphorylation and cytosol-to-nucleus translocation of TFEB (13–15). Then, nuclear TFEB promotes expression of autophagic and lysosomal genes. Besides mTORC1, several other protein kinases also regulate TFEB activity and lysosome biogenesis, including GSK3β, Akt, PERK, and CDK4/6 (16, 17). According to previous studies, S122, S134, S138, S142, S211, and S467 are crucial phosphorylated sites on TFEB (16). As aforementioned, the transcription repressor ZKSCAN3 also regulates lysosome biogenesis and the expression of autophagic/lysosomal genes. Li *et al.* identified the PKCδ-JNK2/p38 axis as a novel signaling pathway to inhibit ZKSCAN3 activity and promote lysosome biogenesis based on the screen of lysosome-enhancing compounds (LYECs) (11). So far, phosphorylation and dephosphorylation of key regulators are the major modifications and regulatory mechanisms of lysosome biogenesis.

Several other types of protein modifications, including acetylation, ubiquitination, palmitoylation, and methylation, occur in a variety of cellular processes. In physiological conditions, histone deacetylases (HDACs) and lysine acetyltransferases (KATs) precisely regulate protein acetylation and maintain cellular homeostasis (18). There are five major categories of HDACs in mammalian cells, including class I, IIA, IIB, III, and IV. Class I (HDAC1/2/3/8) and class III (SIRTs) are located mainly in the nucleus, while class IIA/B (HDAC4/5/6/7/9/10) and class IV (HDAC11) are distributed in both cytosol and nucleus (18).

In 2016, Bao *et al.* found that deacetylation of TFEB at K116 promoted lysosome biogenesis (19). However, in 2018, Zhang *et al.* found that acetylation of TFEB at K116 promoted lysosome biogenesis (20). These two contradictory studies raise the scientific question of whether acetylation or deacetylation is required for TFEB activation and nuclear translocation during lysosome biogenesis. In 2020, Wang *et al.* found that

[‡] These authors contributed equally to this work.
* For correspondence: Yang Li, oceanyangli@fudan.edu.cn.

acetyltransferase GCN5 promoted acetylation of nuclear TFEB at K274 and K279, which disrupts the dimerization and transcriptional activity of TFEB (21). Notably, none of these studies explored whether acetylation/deacetylation of TFEB is dependent or independent of TFEB phosphorylation/dephosphorylation during lysosome biogenesis. Another important question is whether the activities of HDACs or KATs are related to the mTORC1 or GSK3β signaling pathways during TFEB nuclear translocation.

In this study, we report that TFEB acetylation, as a novel modification of TFEB, promotes cytosol-to-nucleus translocation of TFEB and lysosome biogenesis independently of TFEB dephosphorylation. We also identify novel acetylated sites and the related HDACs and KATs, which regulate TFEB acetylation and nuclear translocation during lysosome biogenesis. Notably, administration of the HDAC inhibitor Trichostatin A (TSA) increases the expression of lysosomal genes and promotes the clearance of amyloid β (Aβ) aggregates in APP/PS1 mouse brains, which subsequently improves the memory of those mice. In conclusion, our results provide evidence that TFEB acetylation, as a novel mechanism promoting lysosome biogenesis, alleviates the pathogenesis of AD and could be a potential therapeutic approach for neurodegenerative diseases and disorders related to HDAC hyperactivation.

Results

TSA promotes nuclear translocation of TFEB and lysosome biogenesis

To uncover novel mechanisms of TFEB regulation and lysosome biogenesis, we performed a screen of LYECs in HeLa cells stably expressing TFEB-EGFP. Interestingly, we found that TSA, the pan-inhibitor of HDACs, significantly promoted nuclear translocation of TFEB-EGFP in dose- and time-dependent manners (Fig. 1, *A*–*C*). Torin1, an inhibitor of mTORC1, was used to promote TFEB nuclear translocation as a positive control (Fig. 1, *B* and *C*). We also found that TSA treatment induced translocation of endogenous TFEB from the cytosol into the nucleus (Fig. 1, *D* and *E*). Next, we found that TSA enhanced the staining of cells by LysoTracker Red, a fluorescent lysosomal probe, as measured by flow cytometry (Fig. 1, *F* and *G*). In addition, we also found that TSA upregulated the immunostaining and protein level of endogenous lysosomal associated membrane protein 1 (LAMP1), a membrane marker of lysosomes (Fig. S1, *A* and *B*). These results suggested that TSA increased the number of lysosomes and promoted lysosome biogenesis. Further, TSA treatment also enhanced the staining of BODIPY pepstatin A, which binds with active cathepsin D within lysosomal lumen (Fig. 1, *H* and *I*). The colocalization of BODIPY pepstatin A and LysoTracker Red was enhanced by TSA, suggesting that the new lysosomes were mature and functional (Fig. 1, *H* and *I*). As a transcription factor, TFEB promotes the expression of autophagic and lysosomal genes. Therefore, we examined the expression of TFEB target genes. After TSA treatment, the expression of lysosomal and autophagic genes was elevated significantly (Fig. 1, *J* and *K*). This effect of TSA on autophagic and lysosomal genes was dependent on TFEB activation, since TFEB deficiency prevented the TSA-induced increase in expression of these genes (Figs. 1, *L*, *M*, S1, *C* and *D*). Thus, TSA promotes nuclear translocation of TFEB and lysosome biogenesis. Similarly, SAHA, another pan-inhibitor of HDACs, also significantly promoted nuclear translocation of TFEB-EGFP and increased the expression of lysosomal and autophagic genes (Fig. S1, *E*–*G*)

TSA induces acetylation of TFEB

Since TSA is a pan-inhibitor of HDACs, we speculated that TSA treatment may influence the acetylation of TFEB. After treating cells with TSA, we performed immunoprecipitation of TFEB-EGFP and examined TFEB acetylation using an antibody against acetyl-lysine. We found that acetylation of TFEB-EGFP was significantly enhanced in TSA-treated cells, compared to dimethyl sulfoxide (DMSO)–treated ones (Fig. 2, *A* and *B*). However, Torin1 did not increase the acetylation of TFEB-EGFP during Torin1-induced TFEB nuclear translocation and activation (Fig. S2*A*). Notably, the protein levels of both TFEB-EGFP and endogenous TFEB were robustly elevated after TSA treatment (Fig. 2, *A* and *C*). This effect of TSA on the protein levels of TFEB occurred in a time-dependent manner (Fig. 2, *C* and *D*). Importantly, TSA also induced nuclear translocation and acetylation of TFE3 (Fig. S2, *B*–*E*).

Then, we identified potential acetylation sites in the TFEB protein sequence using prediction software, namely PAIL (Prediction of Acetylation on Internal Lysines). We chose the sites with the top 10 highest scores and created single point mutations (K to Q, or K to R) to dissect the relationship between TFEB acetylation and its nuclear translocation. We found that point mutations of four sites—K116Q, K236Q, K237Q, and K431Q—mimicked TSA-induced TFEB acetylation and nuclear translocation (Fig. 2*E*). We also made constructs expressing double (K236/237Q), triple (K116/236/237Q or K236/237/431Q), and multiple mutations (K116/236/237/431Q) of TFEB-EGFP. Overexpression of these mutants also mimicked TSA-induced nuclear translocation of TFEB, which revealed that all four of these sites are important for TFEB acetylation and nuclear translocation (Fig. 2*F*). Furthermore, the acetylation of TFEB at K116, K236/K237, and K431 was detected by mass spectrometry (Fig. S3).

To confirm that the acetylation of the aforementioned four sites is required for TFEB nuclear translocation and lysosome biogenesis induced by TSA treatment, we made the mutant TFEB-EGFP(4KR), in which K116/236/237/431 are changed to R, to mimic the deacetylation of TFEB. We observed that TFEB-EGFP(4KR) reversed TSA-induced nuclear translocation compared with TFEB-EGFP(WT) (Fig. 2, *G* and *H*). Importantly, K236 and K237 localize in the nuclear localization signal (NLS) region of TFEB, and we found that TSA significantly reduced the binding between 14-3-3 and TFEB, while K236R/K237R reversed TSA-declined binding between 14-3-3 and TFEB, which indicated that deacetylation of K236 and K237 could mask an NLS in TFEB (Fig. S4, *A*–*C*). Torin1

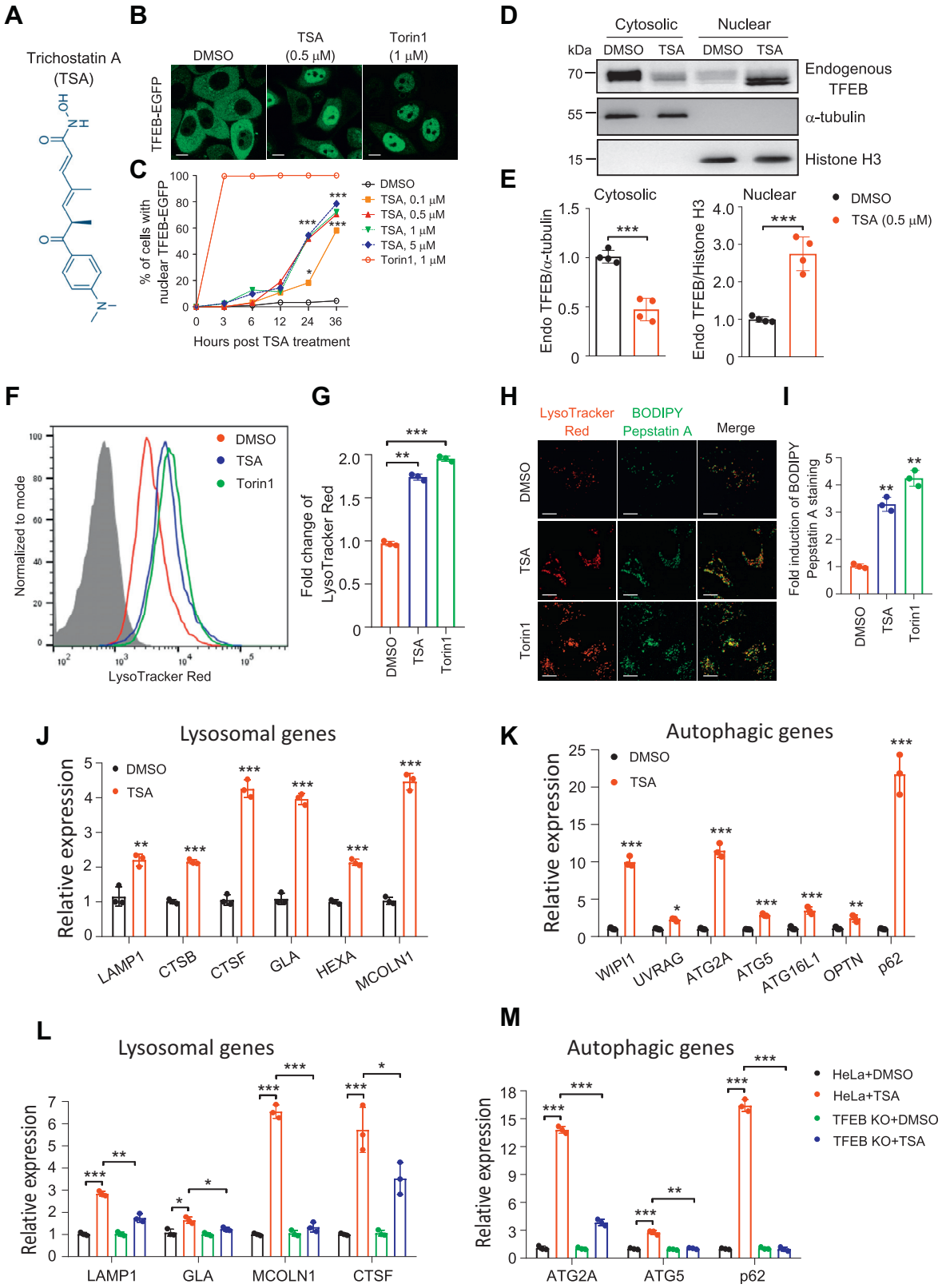

Figure 1. TSA induces TFEB-dependent lysosome biogenesis. *A*, chemical structure of TSA. *B* and *C*, TSA induces nuclear translocation of TFEB-EGFP in a dose- and time-dependent manners. HeLa cells were treated with TSA or Torin1 for the indicated time and then nuclear translocation of TFEB-EGFP was observed and calculated. DMSO, dimethyl sulfoxide. For the quantification, three independent experiments were performed. The scale bars represent 10 μm. *D* and *E*, immunoblot analysis of endogenous TFEB in the cytosol and nucleus of HeLa cells after TSA treatment (0.5 μM, 12 h). α-tubulin and Histone H3 were used as quality controls for the cytosolic and nuclear fractions, respectively. Blot images are from one experiment that is representative of four independent experiments. *F* and *G*, TSA enhances the staining of LysoTracker Red. Quantifications of lysosomes (fold induction of LysoTracker staining) of HeLa cells treated with TSA (0.5 μM, 24 h) or Torin1 (1 μM, 6 h) are shown. n = 3 independent experiments. *H* and *I*, images and quantifications of HeLa cells treated with TSA (0.5 μM, 24 h) or Torin1 (1 μM, 6 h) and costained with BODIPY-pepstatin A (1 μM) and LysoTracker Red (0.3 μM). n = 3 independent

was used as a positive control. Accordingly, using the acetyl-lysine antibody, we found that TFEB-EGFP (2KR, 3KR, or 4KR) also significantly attenuated TSA-induced acetylation of TFEB compared with TFEB-EGFP(WT) after TSA treatment (Fig. 2, *I* and *J*). Importantly, overexpression of TFEB-EGFP(4KR) in TFEB-deficient cells reversed the TSA-induced elevation in expression of lysosomal and autophagic genes (Fig. 2*K*). TSA still increased the expression of lysosomal and autophagic genes in TFEB KO cells overexpressing TFEB-EGFP(WT) (Fig. 2*K*). However, unlike TSA treatment, Torin1 promoted nuclear translocation of both WT and mutant TFEB-EGFP (2KR, 3KR, or 4KR) in TFEB KO cells (Fig. S4, *D* and *E*). This indicates that deacetylation of these four sites did not affect TFEB dephosphorylation and activation induced by mTORC1 inhibition. Taken together, our results show that TSA promotes the acetylation of TFEB at K116, K236, K237, and K431, which is required for nuclear translocation of TFEB and lysosome biogenesis.

HDACs and KATs regulate TFEB nuclear translocation and lysosome biogenesis

Protein acetylation is precisely regulated by HDACs and KATs (18). Since TFEB is translocated from the cytosol into the nucleus after TSA-mediated HDAC inhibition, we wondered which cytosolic HDAC and/or KAT participated in the regulation of TFEB acetylation and translocation. Firstly, we knocked down cytosol-localized HDACs (class IIA, IIB, and IV) using specific siRNAs and found that knockdown of HDAC5 and/or HDAC9 strongly promoted nuclear translocation of TFEB-EGFP (Figs. 3, *A*, *B*, and S1*H*). Knockdown of HDAC6 also promoted TFEB nuclear translocation, but the magnitude was less than knockdown of HDAC5 or HDAC9 (Figs. 3, *A*, *B*, and S1*H*). Accordingly, siHDAC(5 + 9) enhanced the staining of cells by LysoTracker Red compared with the staining in cells after siCtrl treatment (Fig. S5, *A* and *B*). Consistent with these results, SB939, a specific inhibitor of HDAC5 and HDAC9, significantly promoted TFEB nuclear translocation and increased the expression of lysosomal and autophagic genes (Fig. S1, *E*, *I*, and *J*). To identify which acetylation sites on TFEB are regulated by HDAC5/9, we examined the nuclear translocation of TFEB(WT) and TFEB(4KR) in siHDAC cells. After siHDAC(5 + 9) treatment, the 4KR mutant of TFEB-EGFP was resistant to translocation into the nucleus compared with WT TFEB-EGFP (Fig. 3, *C* and *D*). These results demonstrated that inhibition of HDAC5 and HDAC9 promote nuclear translocation of TFEB and enhance lysosome biogenesis.

Secondly, we wanted to identify the KATs participating in TFEB acetylation and lysosome biogenesis. We searched the literature for cytosolic KATs and then purchased a specific KAT shRNA library, which is commercially available (Fig. S6, *A* and *E*). After transfection of library constructs into cells, expression of shRNAs is induced by tetracycline (doxycycline, Dox) treatment, then RFP signals are observed in the transfected cells (Fig. S6*B*). We confirmed that Dox treatment did not affect TFEB nuclear translocation without or with TSA (Fig. S6, *C* and *D*). When we screened the library, we found that knockdown of ELP3 by two different ELP3 shRNAs, either separately (B2 or C3) or combined together (B2 + C3), reversed TSA-induced nuclear translocation of TFEB-EGFP (Figs. 3, *E* and *F*, and S7*A*). Consistent with this, overexpression of Flag-ELP3 enhanced the staining by LysoTracker Red (Fig. S5, *C* and *D*). In addition, overexpression of Flag-tagged ELP3 promoted nuclear translocation of WT TFEB-EGFP, and the combination of Flag-ELP3 transfection and TSA treatment further enhanced TFEB nuclear translocation (Fig. 3, *G* and *H*). However, overexpression of Flag-ELP3 did not promote nuclear translocation of the TFEB-EGFP(4KR) mutant, which suggests that ELP3 affects TFEB translocation by regulating TFEB acetylation at these four sites.

When we screened the shRNA library specific to cytosolic KATs, we also observed that knockdown of another two KATs, CREBBP or HAT1, reversed TSA-promoted nuclear translocation of TFEB-EGFP (Figs. S6*E*, and S7, *B*–*G*). This result indicates that CREBBP and HAT1 also regulate TFEB nuclear translocation during lysosome biogenesis.

TFEB acetylation is regulated by HDAC5/9 and ELP3

Consistent with elevated nuclear translocation of TFEB and enhanced staining of LysoTracker Red, treatment with siHDAC5 and/or siHDAC9 increased TFEB acetylation, as revealed by detection with the acetyl-lysine antibody (Fig. 4*A*). Notably, compared with TFEB(WT), the acetylation of TFEB(4KR) was not increased by siHDAC(5 + 9) treatment (Fig. 4, *A* and *B*), which indicates that HDAC5 and HDAC9 regulate TFEB acetylation at K116, K236/K237, and K431.

Similarly, overexpression of Flag-ELP3 also increased acetylation of TFEB(WT), but not mutant TFEB(4KR) (Fig. 4, *C* and *D*), which indicates that the acetyltransferase ELP3 promotes TFEB acetylation at K116, K236/K237, and K431. Furthermore, we immunoprecipitated ELP3 and purified TFEB (Fig. S8) and then performed an *in vitro* acetylation assay. We found that ELP3 promoted acetylation of TFEB(WT) (Fig. 4, *E* and *F*). However, the mutants of TFEB were resistant to ELP3-mediated acetylation, among which the reversal effect of mutant TFEB (4KR) was the most significant and less mutations of TFEB could not abolish TFEB acetylation (Fig. 4, *E* and *F*). These results demonstrate that ELP3 directly acetylates TFEB at these four sites.

experiments. The scale bars represent 10 μm. *J* and *K*, TSA induces the expression of lysosomal genes (*J*) and autophagic genes (*K*). HeLa cells were treated with TSA (0.5 μM, 24 h) and subjected to qRT-PCR analysis. n = 3 independent experiments. *L* and *M*, the TSA-induced increase in the expression of lysosomal genes (*L*) and autophagic genes (*M*) is dependent on TFEB. HeLa cells and TFEB KO cells were treated with TSA (0.5 μM, 24 h) and subjected to qRT-PCR analysis. n = 3 independent experiments. For all quantifications, data (mean ± SD) were from the indicated number of independent experiments and were analyzed using *t*-tests or ANOVA. $*p < 0.05$, $**p < 0.01$, $***p < 0.001$. DMSO, dimethyl sulfoxide; qRT-PCR, quantitative real-time PCR; TFEB, transcription factor EB; TSA, Trichostatin A.

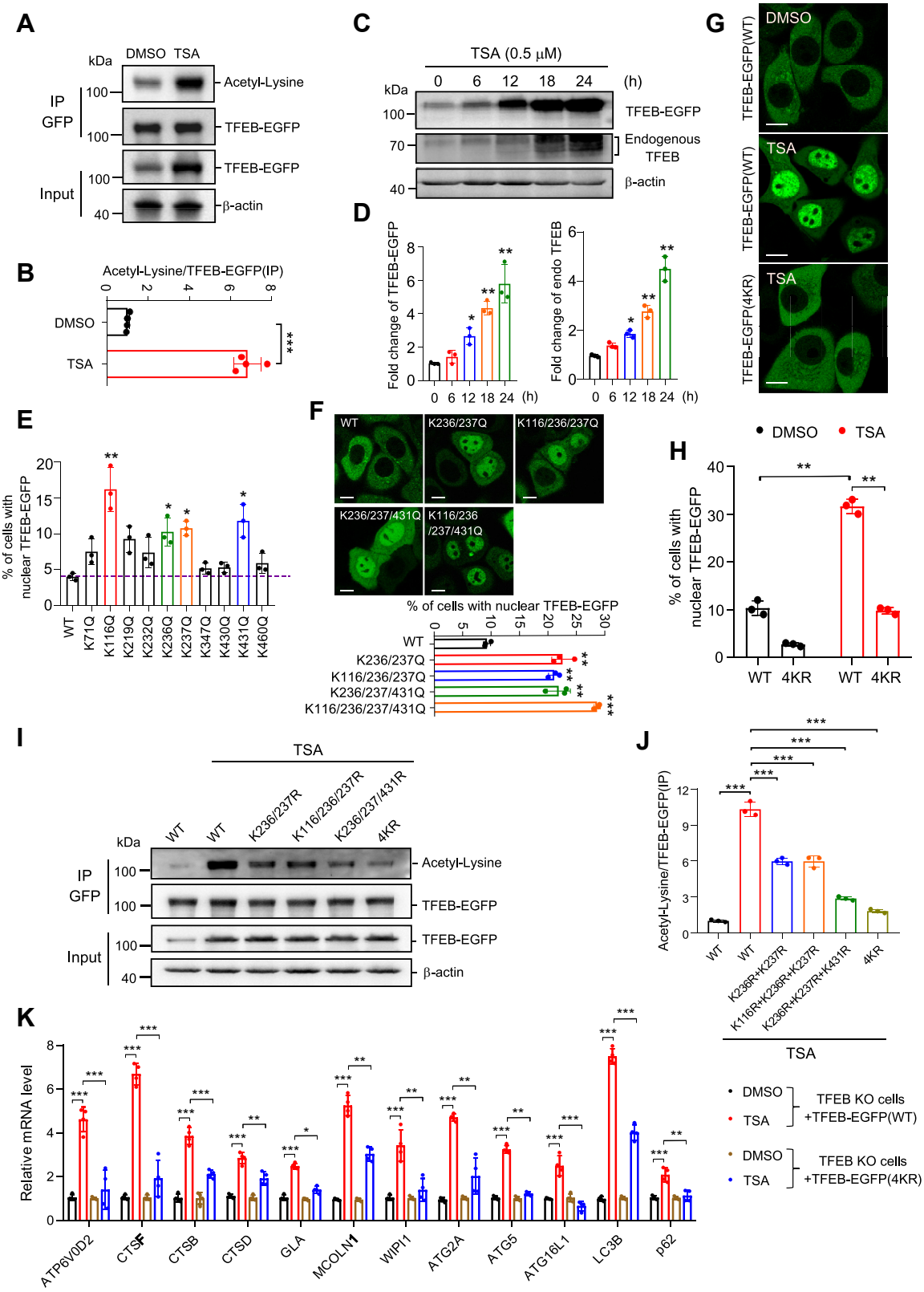

Figure 2. TSA induces TFEB acetylation. *A* and *B*, immunoblotting of acetyl-lysine and TFEB-EGFP (*A*). HeLa cells stably expressing TFEB-EGFP were treated without or with TSA (0.5 μM) for 24 h and immunoprecipitated with GFP-Trap beads. Precipitated proteins were detected with antibodies against acetyl-lysine or GFP. Quantification of acetyl-lysine/TFEB-EGFP is shown in (*B*). The immunoblot image is from one experiment that is representative of four independent experiments. *C* and *D*, TSA increases the protein levels of both TFEB-EGFP and endogenous TFEB in cells with stable expression of TFEB-EGFP. *C*, immunoblotting of TFEB-EGFP, endogenous TFEB, and actin. *D*, fold change of TFEB-EGFP and endogenous TFEB. The immunoblot image is from one experiment that is representative of three independent experiments. *E*, quantification of nuclear localization of TFEB-EGFP with the indicated point mutations (K to Q) in HeLa cells. n = 3 independent experiments. *F*, representative images and quantification of nuclear localization of TFEB-EGFP with the indicated multiple mutations (K to Q) in HeLa cells. n = 3 independent experiments. The scale bars represent 10 μm. *G* and *H*, TFEB-EGFP(4KR) antagonizes

Acetylation and Ubiquitination of TFEB

TFEB acetylation is independent of TFEB dephosphorylation during TSA-induced nuclear translocation of TFEB

Previous studies used inhibition of TFEB-upstream kinases, including mTORC1, GSK3β, and Akt, to show that translocation and activation of TFEB are dependent on its dephosphorylation (16). There are several phosphorylated sites on TFEB, including S122, S134, S138, S142, and S211, whose dephosphorylation is crucial for translocation of TFEB into the nucleus (16). Once these sites are dephosphorylated, TFEB becomes active, then translocates into the nucleus, and subsequently functions as one of the key transcription factors to promote lysosome biogenesis. Since TSA-induced TFEB acetylation occurs at K116, K236/237, and K431, we wanted to examine whether acetylation-induced nuclear translocation of TFEB is dependent or independent of TFEB dephosphorylation. First, we found that TSA treatment did not inhibit mTORC1 activity, since the protein level of p-S6K was not attenuated by TSA (Fig. 5, *A* and *B*). Also, TSA treatment did not significantly affect GSK3β phosphorylation at Ser9, an inhibitory phosphorylation site, which suggests that GSK3β activity was not inhibited by TSA (Fig. 5, *A* and *C*). Accordingly, knockdown of HDACs did not inhibit the activity of mTORC1 or GSK3β (Fig. 5, *D* and *E*). These results suggest that TSA-induced TFEB nuclear translocation might be not dependent on TFEB dephosphorylation.

To confirm that, we performed immunoprecipitation of TFEB-EGFP after TSA treatment and examined changes of TFEB phosphorylation/dephosphorylation by mass spectrometry. Notably, the level of phosphorylation at S122, S134, S138, and S142 did not decline on TFEB from TSA-treated cells compared with TFEB from DMSO-treated cells (Fig. 5*F*). We also made TFEB-EGFP constructs with mutations (S to D) at these four phosphorylation sites to mimic phosphorylated TFEB. The mutants were S122D, S134D/S138D, and S142D. Interestingly, TSA treatment still significantly promoted nuclear translocation of these mutant TFEB-EGFP proteins, similar to the WT TFEB-EGFP (Fig. 5, *G* and *H*). We also found that S211 on TFEB was still phosphorylated after TSA treatment, like in DMSO-treated cells, while Torin1 significantly reduced the phosphorylation at S211 (Fig. 5, *I* and *J*). These results demonstrate that acetylated TFEB was still phosphorylated after TSA treatment. Taken together, the data show that TFEB acetylation is independent of its dephosphorylation during its TSA-induced nuclear translocation.

Increased acetylation and decreased ubiquitination of TFEB occur simultaneously at K347 after TSA treatment

Interestingly, we also found that acetylation of TFEB at K347 was significantly elevated after TSA treatment (Fig. S9, *A* and *C*), even though the mutations (K347Q and K347R) did not affect nuclear translocation of TFEB significantly nor the expression of lysosomal and autophagic genes without or with TSA treatment (Figs. 2*E* and S9, *D*–*G*). Meanwhile, ubiquitination of TFEB at K347 was significantly decreased after TSA treatment (Fig. S9, *A* and *B*). This change of modifications at the same lysine might be the reason why TSA treatment resulted in a downward shift of TFEB bands on Western blots accompanied by an increased protein level of TFEB (Figs. 1*D*, 2, *A* and *C*).

To examine the ubiquitination of TFEB, we performed immunoprecipitation of TFEB-EGFP after DMSO or TSA treatment. Using the specific antibodies, we found that TSA treatment significantly decreased the ubiquitination of TFEB-EGFP compared with TFEB-EGFP in DMSO-treated cells (Fig. 6, *A* and *B*). This result is consistent with TSA-elevated protein level of TFEB shown in Figure 2*C* and TSA-decreased ubiquitination of TFEB revealed by mass spectrometry in Fig. S9, *A* and *B*. Then, we found that the levels of ubiquitinated TFEB proteins in the TSA-treated cells contained predominantly K48-linked Ub chains (K48-Ub) instead of K63-linked Ub chains (K63-Ub) (Fig. 6, *C*–*F*). In Fig. S9, *A* and *B*, the ubiquitination of TFEB proteins occurred at K347 revealed by mass spectrometry. Notably, we found that the ubiquitination or K48-Ub of TFEB (K347R) was much less than that of TFEB(WT) (Fig. 6, *G*–*J*). Taken together, all these results indicated that the ubiquitination at K347 on TFEB linked to the subsequential proteasomal degradation.

TSA-induced lysosome biogenesis alleviates AD in APP/PS1 mice

Next, we wondered whether TSA-induced TFEB activation and lysosome biogenesis could promote degradation of protein aggregates and ameliorate the pathogenesis of AD. Thus, we intraperitoneally injected TSA into 5-month-old APP/PS1 mice (an animal model of AD) every other day for 1 month until the mice were 6 months old. As shown in Fig. S10, *A* and *B*, we detected certain concentrations of TSA in both heart plasma and brain after i.p. administration, which indicated that TSA could pass through the blood–brain barrier. Besides, the body weights of the TSA-injected APP/PS1 mice were not obviously changed compared with aged-matched vehicle-injected controls and WT mice (Fig. S10*C*). We evaluated the effects of TSA in three ways. Firstly, we found that the Aβ plaques in APP/PS1 mouse brains were significantly ameliorated in both the hippocampus and cortex after TSA injection (Fig. 7, *A*–*C*). TSA reduced the Aβ load by 62.8% in the cortex and 71.3% in the hippocampus compared with age-matched vehicle-injected controls (Fig. 7, *B* and *C*). Aβ42

TSA-induced nuclear translocation. Representative images of TFEB-EGFP translocation in cells without or with TSA (0.5 μM, 20 h) are shown in (*G*) and quantifications are shown in (*H*). n = 3 independent experiments. The scale bars represent 10 μm. *I* and *J*, mutations (K to R) of TFEB-EGFP significantly decrease the acetylation of TFEB-EGFP. Cells were transfected with constructs expressing WT or mutant TFEB-EGFP as indicated, then treated without or with TSA (0.5 μM, 12 h), and immunoprecipitated with GFP-Trap beads. Precipitated proteins were detected with antibodies specific to acetyl-lysine and GFP (*I*). Quantifications of acetyl-lysine/TFEB-EGFP are shown in (*J*). The immunoblot image is from one experiment that is representative of three independent experiments. *K*, TSA-induced expression of lysosomal and autophagic genes is dependent on TFEB acetylation at these four sites. TFEB KO cells were transfected with TFEB-EGFP (WT or 4KR), then treated with TSA (0.5 μM, 24 h), and subjected to qPCR experiments. n = 4 independent experiments. For all quantifications, data (mean ± SD) were from the indicated number of independent experiments and were analyzed using *t*-tests or ANOVA. $^{*}p < 0.05$, $^{**}p < 0.01$, $^{***}p < 0.001$. TFEB, transcription factor EB; TSA, Trichostatin A.

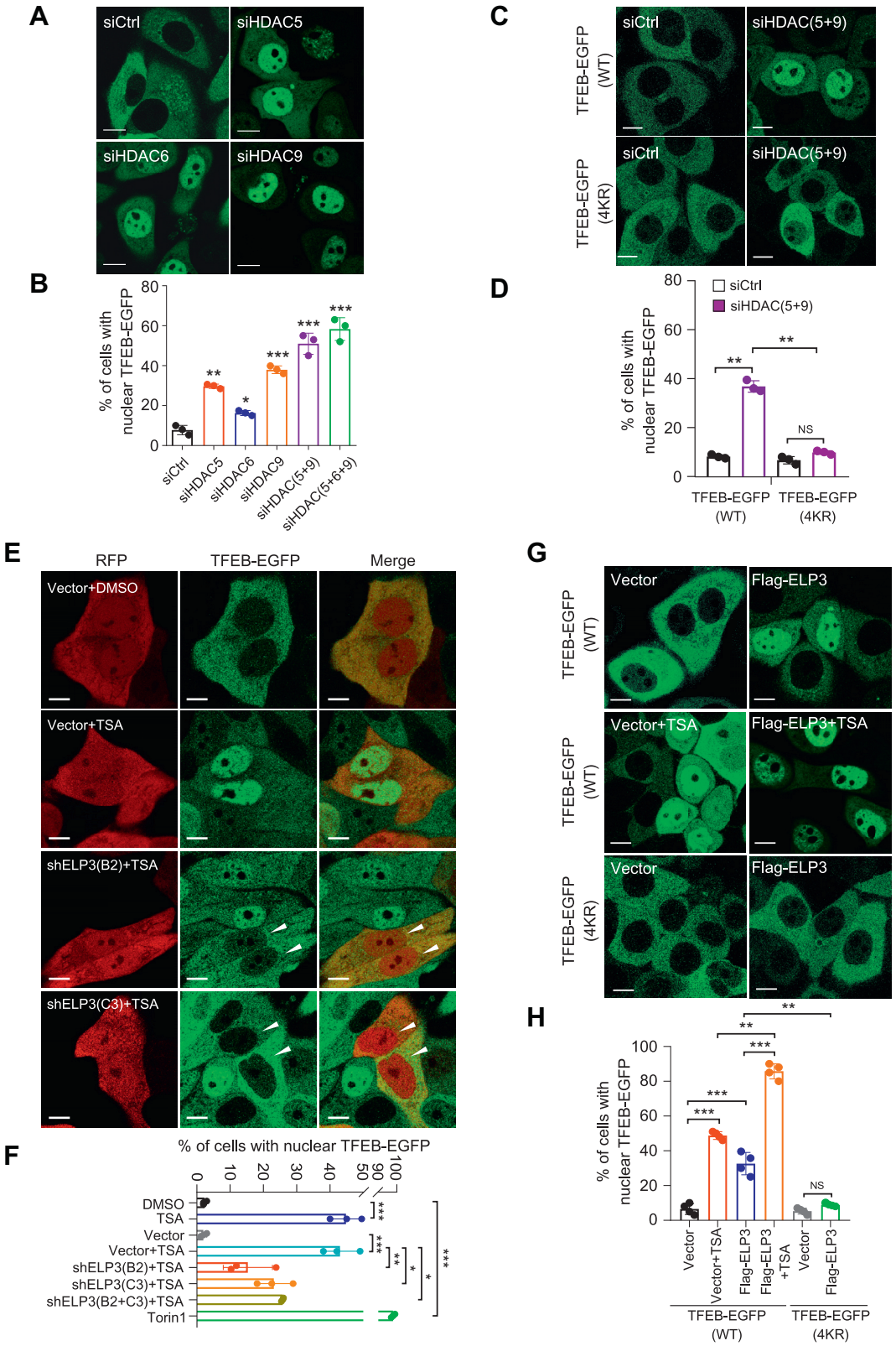

Figure 3. HDAC5/6/9 and ELP3 regulate TFEB nuclear translocation. *A* and *B*, images (*A*) and quantification (*B*) of TFEB-EGFP nuclear translocation induced by specific knockdown of HDAC5, HDAC6, or HDAC9 in HeLa cells. n = 3 independent experiments. The scale bars represent 10 μm. *C* and *D*, TFEB-EGFP(4KR) antagonizes siHDAC(5 + 9)-induced nuclear translocation. HeLa cells were transfected with TFEB-EGFP (WT or 4KR), then treated by siHDAC5 and siHDAC9. Representative images of TFEB-EGFP nuclear translocation (*C*) and quantifications (*D*) are shown. n = 3 independent experiments. The scale bars represent 10 μm. *E* and *F*, two different ELP3 shRNAs (B2 and C3) reverse TSA-induced TFEB-EGFP nuclear translocation. Representative images of TFEB-EGFP nuclear translocation (*E*) and quantifications (*F*) in HeLa cells are shown. HeLa cells were transfected with shELP3, then treated with Dox (1 μM) to induce shRNA expression (RFP is coinduced, so shRNA-positive cells are also RFP-positive). After 12 h, Dox was removed and cells were further cultured in fresh medium containing TSA (0.5 μM) for 24 h. n = 3 independent experiments. The scale bars represent 10 μm. *Arrows*: no nuclear translocation of TFEB-EGFP in

concentrations were decreased by 38.6% in the cortex and 25.6% in the hippocampus, respectively (Fig. 7, *D* and *E*). Secondly, TSA injection significantly upregulated the expression of autophagic and lysosomal genes in APP/PS1 mouse brains (Fig. 7*F*). Thirdly, we performed behavioral experiments, including the Morris Water Maze (MWM) and Y maze tests, to evaluate the effects of TSA treatment on learning, memory and cognitive function of APP/PS1 mice. In the MWM test, APP/PS1 mice injected with TSA took significantly less time to locate the platform and landed on the platform more often when compared to vehicle-injected controls (Figs. 7*G* and S10*D*). During the probe trial, mice injected with TSA crossed the platform more often and spent significantly more time in the target quadrant compared to controls (Figs. 7*H* and S10*E*). And, the performance of APP/PS1 mice was improved after TSA treatment compared to controls in the Y maze test (Fig. 7*I*). Thus, TSA treatment enhanced lysosome biogenesis and Aβ clearance in APP/PS1 mice and improved their learning, memory, and cognitive function.

Discussion

In this study, we demonstrate that TFEB acetylation, as a novel modification of TFEB, promotes TFEB nuclear translocation and lysosome biogenesis independently of TFEB dephosphorylation. HDAC5/9 and ELP3 coordinate TFEB acetylation to maintain the appropriate level of lysosome biogenesis (Fig. 8, *A* and *B*). Comparing TFEB dephosphorylation with acetylation during its nuclear translocation, we observe two patterns of TFEB activation. (1) The process of dephosphorylation-mediated TFEB translocation is acute (within 3 h). It is usually regulated by mTORC1 or PKC-GSK3β signaling for maintenance of cellular homeostasis in response to environmental stresses, including starvation or pathogen invasion. (2) The process of acetylation-mediated TFEB translocation is comparatively slow (almost 24 h). It is regulated by HDACs and KATs in response to pathophysiological cues, including neurodegenerative or metabolic disorders.

Previously, the regulatory mechanisms of TFEB acetylation and activity have already been studied and reported by several groups. Zhang *et al*. reported that SAHA treatment, an inhibitor of HDACs, induced TFEB activation and lysosome biogenesis *via* promoting TFEB acetylation at four sites, including K91, K103, K116, and K430. Consistently, we found that TSA treatment also induced TFEB activation and lysosome biogenesis *via* promoting TFEB acetylation. However, the acetylation sites on TFEB induced by TSA were partially different, including K116, K236, K237, and K431. Although both SAHA and TSA are pan-inhibitors of HDACs, SAHA is more efficient to inhibit HDAC1-3, HDAC6-7, and HDAC11, while TSA is more efficient to inhibit HDAC1-3, HDAC4-7, and HDAC9. Thus, the different patterns of HDAC inhibition result in different acetylation sites on TFEB after SAHA or TSA treatment. Interestingly, Bao *et al*. reported that deacetylation of TFEB at K116 promoted lysosome biogenesis. However, a fibrillar Aβ, as a proteotoxic stress, was used in their study as a pathological stimulation and made complicated to evaluate the effect of SIRT1-mediated TFEB deacetylation on lysosome biogenesis, since the fibrillar Aβ had already induced TFEB nuclear translocation and lysosome biogenesis. During this cellular process, TFEB may have been already acetylated and activated by this proteotoxic stress.

Previous studies have found that HDAC inhibitors modify TFEB acetylation, and another study showed TSA modified behavior in APP/PS1 mice (22). We therefore evaluate mechanisms of HDAC inhibition on TFEB activation and lysosome biogenesis to confirm the findings of the previous *in vivo* study on TSA-induced amelioration of AD. Besides, we also discovered that (1) TFEB acetylation is independent of TFEB dephosphorylation during TFEB nuclear translocation; (2) K236/K237 and K431 are the novel acetylated sites on TFEB. Notably, K236 and K237 localize in the NLS region of TFEB (Fig. 8*B*). The acetylation occurring at these two sites are crucial for unmasking the NLS of TFEB and breaking the binding between TFEB and 14-3-3 proteins (Fig. 8*B*). We also found that both increased acetylation and decreased ubiquitination of TFEB at K347 after TSA treatment, which is important for TFEB protein stability (Fig. 8*B*).

According to our results from mass spectrometry and comparative localization of mutant and WT TFEB, we confirm that TFEB acetylation at K116 is required for TFEB nuclear translocation and lysosome biogenesis. Furthermore, we also identify other novel acetylation sites on TFEB, including K236/K237 and K431. All of these sites are evolutionarily conserved (Fig. S11*A*), and TSA treatment increases the expression of lysosomal genes in both mammalian cells and mouse brains. We searched the BioMuta database to explore whether these acetylation sites on TFEB are related to human diseases. However, there are no reported cases linked to the acetylation sites on TFEB. Interestingly, we found that mutations next to these TFEB acetylation sites, including P115L, E233G, and D432G, are related to melanoma and lung cancers in human patients. These mutations may interrupt the normal processes of TFEB acetylation and lysosome biogenesis, resulting in dysregulation of cellular homeostasis and disease pathogenesis.

Notably, we also identify a novel ubiquitination site on TFEB at K347, which is evolutionarily conserved (Fig. S11*B*). After TSA treatment, acetylation on K347 is increased. Meanwhile, ubiquitination on K347 is decreased. This result explains why the TFEB band shifts downward in Western blotting, since the molecular weight of a polyubiquitin chain is much larger than the molecular weight of an acetyl group. This

the cells transfected with shELP3 (*red*). *G* and *H*, overexpression of Flag-ELP3 promotes nuclear translocation of TFEB-EGFP. HeLa cells were transfected with TFEB-EGFP (WT or 4KR) and Flag-ELP3, then treated without or with TSA (0.5 μM, 12 h). Representative images of TFEB-EGFP nuclear translocation (*G*) and quantifications (*H*) are shown. n = 4 independent experiments. The scale bars represents 10 μm. For all quantifications, data (mean ± SD) were from the indicated number of independent experiments and were analyzed using *t*-tests or ANOVA. $^{*}p < 0.05$, $^{**}p < 0.01$, $^{***}p < 0.001$. HDAC, histone deacetylase; TFEB, transcription factor EB; TSA, Trichostatin A.

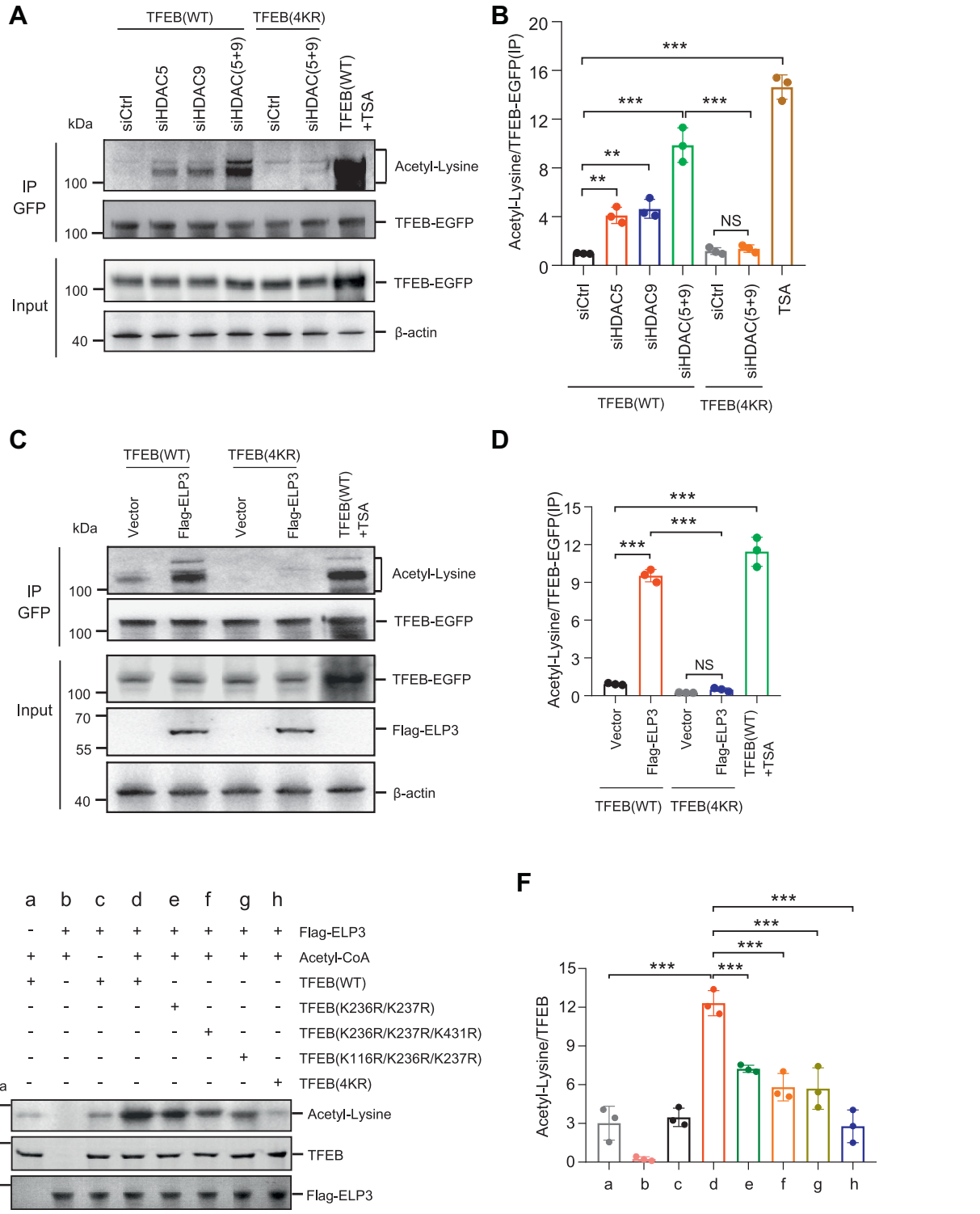

Figure 4. Knockdown of HDAC5 or/and HDAC9 or overexpression of ELP3, promotes TFEB acetylation. *A* and *B*, knockdown of HDAC5 or/and HDAC9 increases TFEB acetylation. TFEB-EGFP (WT or 4KR, 1.5 μg) was transfected into HeLa cells, and the cells were then treated with siCtrl, siHDAC5, siHDAC9, or siHDAC(5 + 9). After immunoprecipitation with GFP-Trap beads, precipitated proteins were detected with antibodies specific to acetyl-lysine or GFP (*A*). Quantifications of acetyl-lysine/TFEB-EGFP are shown in (*B*). The immunoblot image is from one experiment that is representative of three independent experiments. *C* and *D*, overexpression of Flag-ELP3 promotes TFEB acetylation. HeLa cells were cotransfected with TFEB-EGFP (WT or 4KR) and Flag-ELP3. After immunoprecipitation with GFP-Trap beads, precipitated proteins were detected with antibodies specific to acetyl-lysine, GFP, or Flag (*C*). Quantifications of acetyl-lysine/TFEB-EGFP are shown in (*D*). The immunoblot image is from one experiment that is representative of three independent experiments. *E* and *F*, *in vitro* acetylation of TFEB by ELP3. Purified recombinant WT or mutant TFEB was incubated with Flag-ELP3 immunoprecipitated from TFEB KO cells. Precipitated proteins were detected with antibodies specific to acetyl-lysine, TFEB or Flag (*E*). Quantifications of acetyl-lysine/TFEB-EGFP are shown in (*F*). The immunoblot image is from one experiment that is representative of three independent experiments. For all quantifications, data (mean ± SD) were from the indicated number of independent experiments and were analyzed using *t*-tests or ANOVA. *$p < 0.05$, **$p < 0.01$, ***$p < 0.001$. NS, not significant. HDAC, histone deacetylase; TFEB, transcription factor EB.

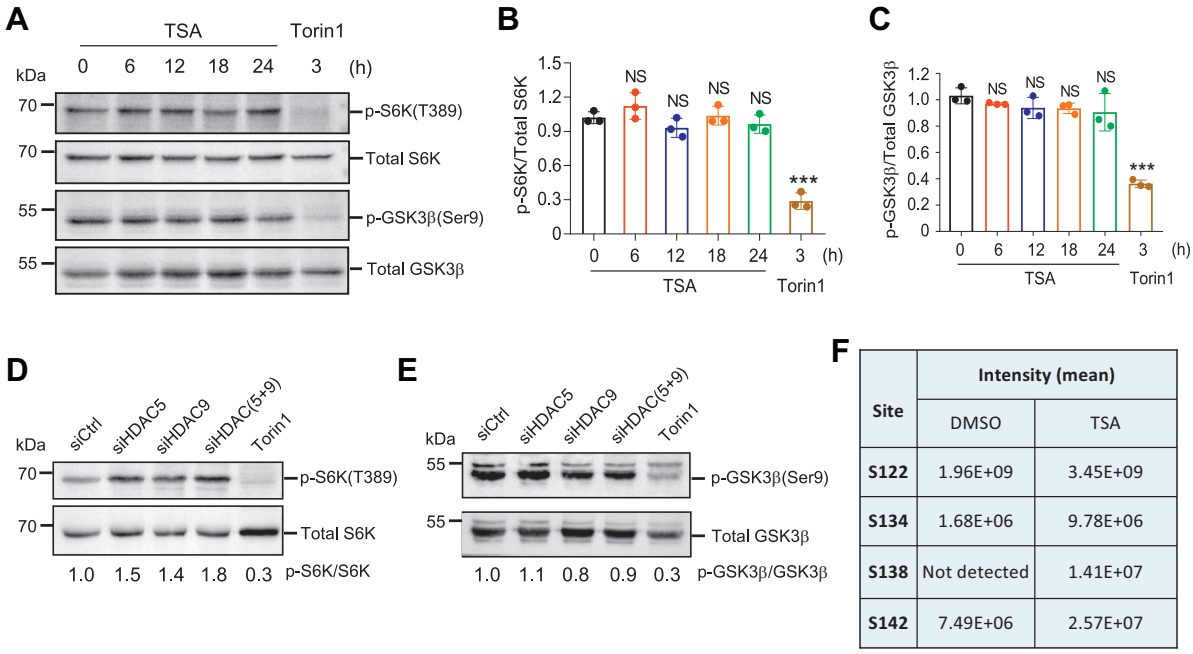

F

Site	Intensity (mean)	
	DMSO	TSA
S122	1.96E+09	3.45E+09
S134	1.68E+06	9.78E+06
S138	Not detected	1.41E+07
S142	7.49E+06	2.57E+07

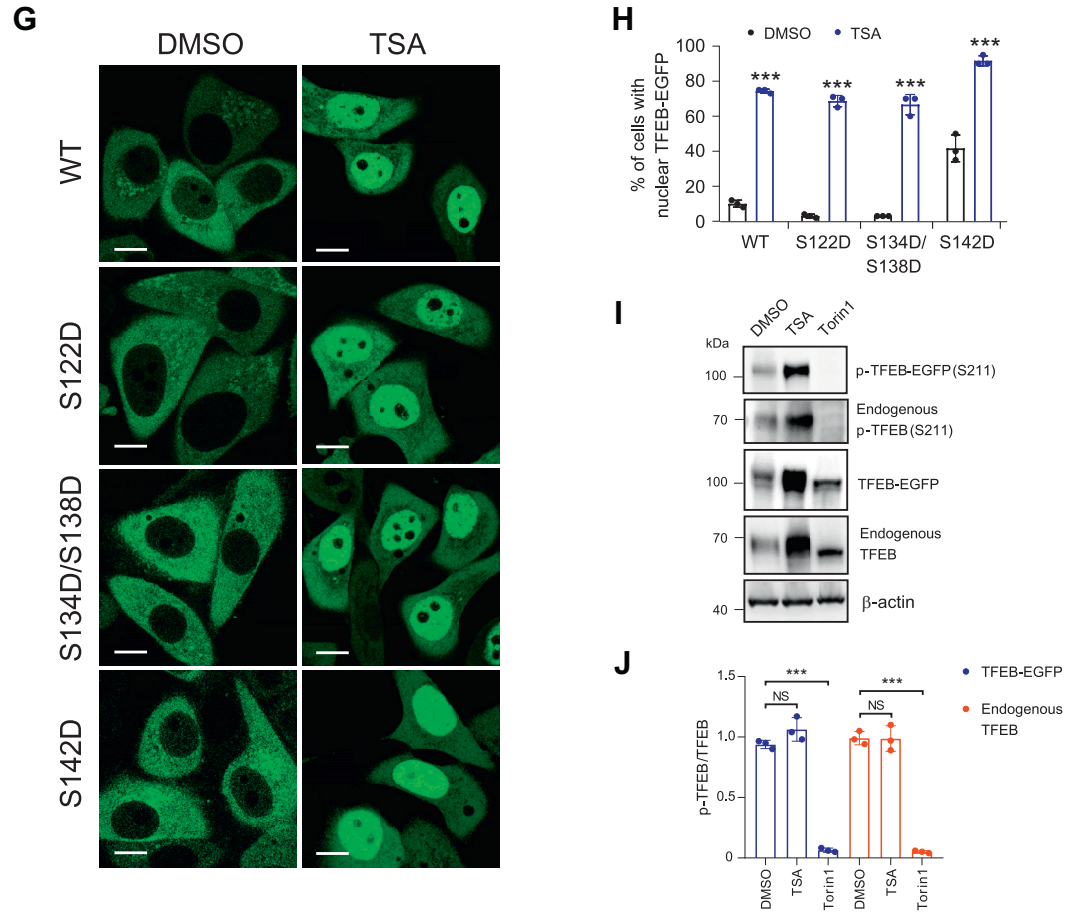

Figure 5. TSA-induced TFEB acetylation and nuclear translocation are independent of TFEB dephosphorylation. *A–C*, immunoblotting of S6K phosphorylation (T389) and GSK3β phosphorylation (Ser9) in HeLa cells treated with TSA (0.5 μM) or Torin1 (1 μM) for the indicated time (*A*). Quantifications of phosphorylated S6K/total S6K are shown in (*B*). Quantifications of phosphorylated GSK3β/total GSK3β are shown in (*C*). The immunoblot image is from one experiment that is representative of three independent experiments. *D*, immunoblot analysis of S6K phosphorylation in HeLa cells treated with siHDAC5 and/or siHDAC9. The fold changes in phosphorylated S6K (T389) are indicated at the bottom. Data are from one experiment that is representative of three independent experiments. *E*, immunoblot analysis of GSK3β phosphorylation in HeLa cells treated with siHDAC5 and/or siHDAC9. The fold changes in phosphorylated GSK3β (Ser9) are indicated at the *bottom*. Data are from one experiment that is representative of three independent experiments. *F*, mass spectrometry analysis of phosphorylation intensity at S122, S134, S138, and S142 on TFEB without or with TSA treatment (0.5 μM, 12 h). *G* and *H*,

result also explains why the protein level of TFEB is increased after TSA treatment, since decreased TFEB ubiquitination at K347 should help the TFEB protein to avoid proteosome-mediated degradation.

We showed here that cytosolic HDAC5/6/9 participate in modification of TFEB and lysosome biogenesis. However, we do not exclude the possibility that nuclear HDACs could also regulate TFEB modification and lysosome biogenesis. A previous study showed that nuclear export of HDAC1 is a critical event for impaired mitochondrial transport and axonal damage in neurons under pathological conditions (23). Therefore, inhibition of cytosolic HDAC1 by TSA may result in TFEB acetylation and enhancement of lysosome biogenesis, which in turn promotes lysosomal-dependent clearance of dysfunctional mitochondria and alleviates axonal damage in neurons.

Studies from other groups have demonstrated that hyperactivation of HDACs induces neural dysfunction, neuron loss, and brain disorders (23–26). HDAC1 promotes TDP-43 deacetylation and aggravates TDP-43 toxicity in ALS models (23). HDAC2 negatively regulates mouse memory formation and synaptic plasticity (24). HDAC6 impairs vesicular transport of brain-derived neurotrophic factor (BDNF) and induces NLRP3 inflammatory responses in models of Huntington's disease and Parkinson's diseases, respectively (25, 26). Thus, inhibition of HDACs not only reverses HDAC-induced damage but also promotes TFEB-dependent lysosome biogenesis to restore neuron homeostasis and brain functions (Fig. S11*C*).

On the other hand, dysfunction of KATs also results in neural abnormalities and brain disorders (27–30). Depletion of ELP3 reduces the level of the modified tRNA wobble uridine mcm^5s^2U and increases the abundance of insoluble mutant SOD1 in an ALS zebrafish model (27). Interestingly, ELP3 expression in the motor cortex of ALS patients is reduced and correlated with levels of mcm^5s^2U (27). Furthermore, knockdown of ELP3 in zebrafish embryos results in dose-dependent motor axonal abnormalities (28). Loss of CREBBP is observed in two pathological contexts, amyloid precursor protein-dependent signaling, and ALS model mice, which indicates that dysfunction of CREBBP is likely to contribute to neurodegenerative diseases (29, 30). These studies suggest to us that KAT dysfunction-induced pathogenesis could also be partially due to dysregulation of lysosome biogenesis. Restoring KAT function may promote lysosome biogenesis, which will subsequently enhance autophagic clearance of protein aggregates and alleviate neurodegenerative diseases (Fig. S11*C*).

Recently, a study, entitled as "Trichostatin A ameliorates Alzheimer's disease-related pathology and cognitive deficits by increasing albumin expression and Aβ clearance in APP/PS1 mice," reported that TSA promoted phagocytosis of Aβ to ameliorate AD-related pathology and cognitive deficits in APP/PS1 mice (22). And, our study found TSA promoted TFEB-mediated lysosome biogenesis and lysosomal degradation of Aβ to ameliorate AD-related pathology and cognitive deficits in APP/PS1 mice. Combination of these two studies facilitates us to understand the roles of HDAC inhibition in the therapeutic approaches of neurodegenerative diseases.

In summary, our study suggests that lysosome biogenesis can be induced by HDAC inhibition, and this is a potential therapeutic approach for the treatment of neurodegenerative diseases and disorders related to HDAC hyperactivity or dysregulation of acetylation.

Experimental procedures

Cell lines and cell culture

All cell lines were cultured in Dulbecco's modified Eagle's medium (DMEM; Gibco) supplemented with 10% fetal bovine serum (Biological Industries), 100 U ml^{-1} penicillin, and 100 mg ml^{-1} streptomycin at 37 °C with 5% CO_2. Control cells and TFEB KO HeLa cells were gifts from Dr Richard Youle's lab in NINDS.

Inhibitors and reagents

The reagents and inhibitors used in this study are listed in Table S1. Unless otherwise stated, inhibitors were used as follows: Torin1 (1 μM, 3 h); TSA (0.5 μM, 24 h); Dox (1 μM, 12 h), SAHA (10 μM, 30 h); SB939 (1 μM, 30 h).

Antibodies

The antibodies used in this study are listed in Table S2.

The screen of LYECs that induce nuclear translocation of TFEB-EGFP

The small molecules used in this study were purchased from Selleck (Natural Product Screening Library (96-well)-Z273329-30 μL-L1400). There are 18 compounds were positive in 192 compounds (#L1400-01). The investigators were blinded to compound identities during this screen. TFEB-EGFP stable cell lines with ∼80% confluency in 24-well plates were treated with indicated compounds at 1 μM, 5 μM, 10 μM, 30 μM, or Torin1 (1 μM). Three or six hours later, nuclear translocation of TFEB-EGFP was examined and analyzed by fluorescent microscopy (Nikon). For the staining of LysoTracker Red (DND-99), cells were grown in DMEM medium containing this probe (0.3 μM) for 0.5 h. Then, cells were changed again to fresh medium and analyzed by flow cytometry (Beckman).

Lysosome quantification by confocal microscopy and flow cytometry

The fluorescence intensity of endogenous LAMP1 was examined with a confocal microscopy (CarlZeiss LSM710).

representative images (*G*) and quantifications (*H*) of TFEB-EGFP nuclear translocation. HeLa cells were transfected with constructs expressing WT or mutant TFEB-EGFP as indicated, then treated with or without TSA (0.5 μM, 12 h). n = 3 independent experiments. The scale bars represent 10 μm. *I* and *J*, immunodetection of TFEB phosphorylation at S211. *I*, cells stably expressing TFEB-EGFP or HeLa cells were treated with TSA (0.5 μM, 12 h) or Torin1(1 μM, 3 h). Exogenous and endogenous TFEB and phosphorylated TFEB (S211) were detected by immunoblotting. *J*, quantifications of phosphorylated TFEB-EGFP/total TFEB-EGFP. For all quantifications, data (mean ± SD) were from the indicated number of independent experiments and were analyzed using *t*-tests or ANOVA. ***$p < 0.001$. NS, not significant. HDAC, histone deacetylase; TFEB, transcription factor EB; TSA, Trichostatin A.

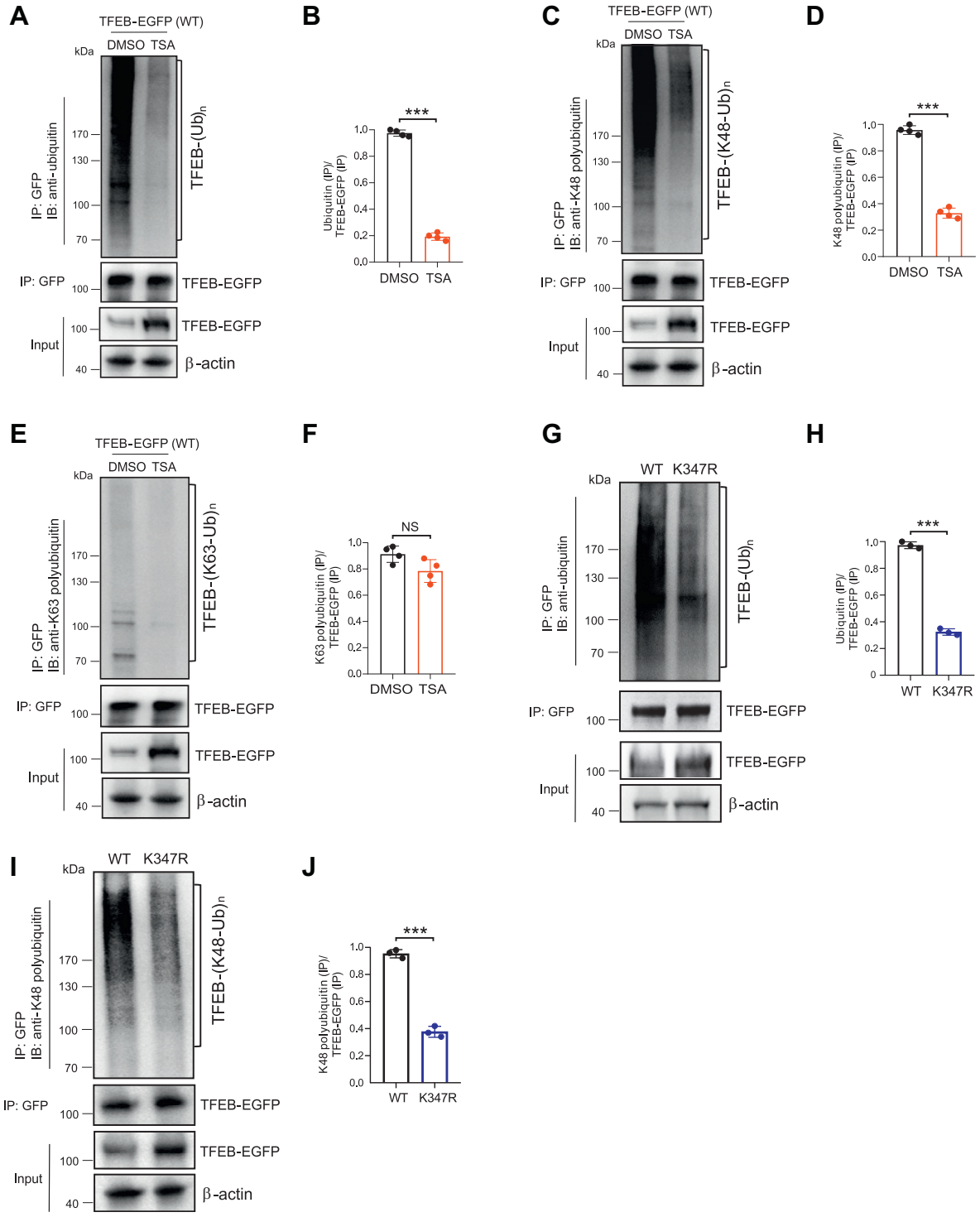

Figure 6. TSA reduced ubiquitination of TFEB. *A* and *B*, immunoblotting of ubiquitination of TFEB-EGFP. HeLa cells stably expressing TFEB-EGFP were treated without or with TSA (0.5 μM) for 24 h and immunoprecipitated with GFP-Trap beads. Precipitated proteins were detected with antibodies against ubiquitin or GFP. Quantification is shown in (*B*). The immunoblot image is from one experiment that is representative of four independent experiments. *C* and *D*, immunoblotting of K48-Ub of TFEB-EGFP. HeLa cells stably expressing TFEB-EGFP were treated without or with TSA (0.5 μM) for 24 h and immunoprecipitated with GFP-Trap beads. Precipitated proteins were detected with antibodies against K48-Ub or GFP. Quantification is shown in (*D*). The immunoblot image is from one experiment that is representative of four independent experiments. *E* and *F*, immunoblotting of K63-Ub of TFEB-EGFP. HeLa cells stably expressing TFEB-EGFP were treated without or with TSA (0.5 μM) for 24 h and immunoprecipitated with GFP-Trap beads. Precipitated proteins were detected with antibodies against K63-Ub or GFP. Quantification is shown in (*F*). The immunoblot image is from one experiment that is representative of four independent experiments. *G* and *H*, immunoblotting of ubiquitination of WT or mutant TFEB-EGFP. HeLa cells transiently expressing TFEB-EGFP(WT) or TFEB-EGFP(K347R) and immunoprecipitated with GFP-Trap beads. Precipitated proteins were detected with antibodies against Ub or GFP. Quantification is shown in (*H*). The immunoblot image is from one experiment that is representative of three independent experiments. *I* and *J*, immunoblotting of K48-Ub of WT or mutant TFEB-EGFP. HeLa cells transiently expressing TFEB-EGFP(WT) or TFEB-EGFP(K347R) and immunoprecipitated with GFP-Trap beads. Precipitated proteins were detected with antibodies against K48-Ub or GFP. Quantification is shown in (*J*). The immunoblot image is from one experiment that is representative of three independent experiments. For all quantifications, data (mean ± SD) were from three independent experiments and were analyzed using *t*-tests. *$p < 0.05$, **$p < 0.01$, ***$p < 0.001$. TFEB, transcription factor EB; TSA, Trichostatin A.

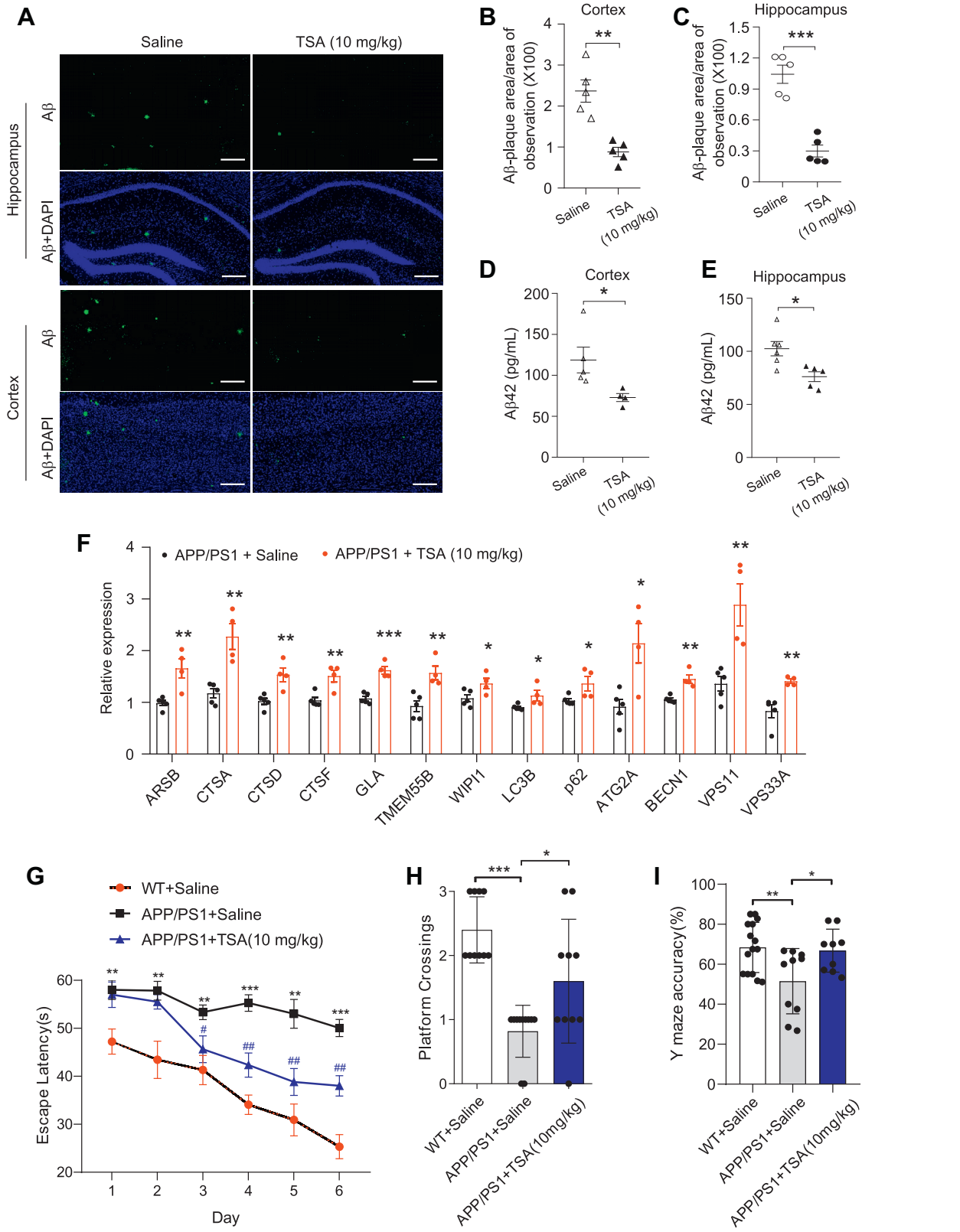

Figure 7. TSA induces a reduction of Aβ plaques in APP/PS1 mouse brains and improves the memory of APP/PS1 mice. *A*, representative images of the hippocampus and cortex of APP/PS1 mouse brain sections immunostained with Aβ antibody (*upper row*) and costained with Aβ antibody and DAPI (*lower row*). Mice were injected with TSA (10 mg/kg) or saline alone. Data are from one mouse that is representative of five mice in each treatment group. The scale bars represent 200 μm. *B* and *C*, quantification of cortical (*B*) and hippocampal (*C*) Aβ plaques in APP/PS1 mice treated with either TSA (n = 5 mice) or saline (n = 5 mice). *D* and *E*, quantification of cortical (*D*) and hippocampal (*E*) Aβ42 levels in APP/PS1 mice treated with either TSA (cortex, n = 4 mice; hippocampal, n = 5 mice) or saline (cortex, n = 5 mice; hippocampal, n = 6 mice). *F*, the expression of autophagic and lysosomal genes in the brains of APP/PS1 mice treated with either TSA (n = 4 mice) or saline (n = 5 mice). Comparisons were made between saline and TSA treatment. *G* and *H*, the escape latency time (*G*) and the number of platform-site crossovers (*H*) in the Morris Water Maze (MWM) test (WT + saline, n = 10 mice; APP/PS1 + saline, n = 11

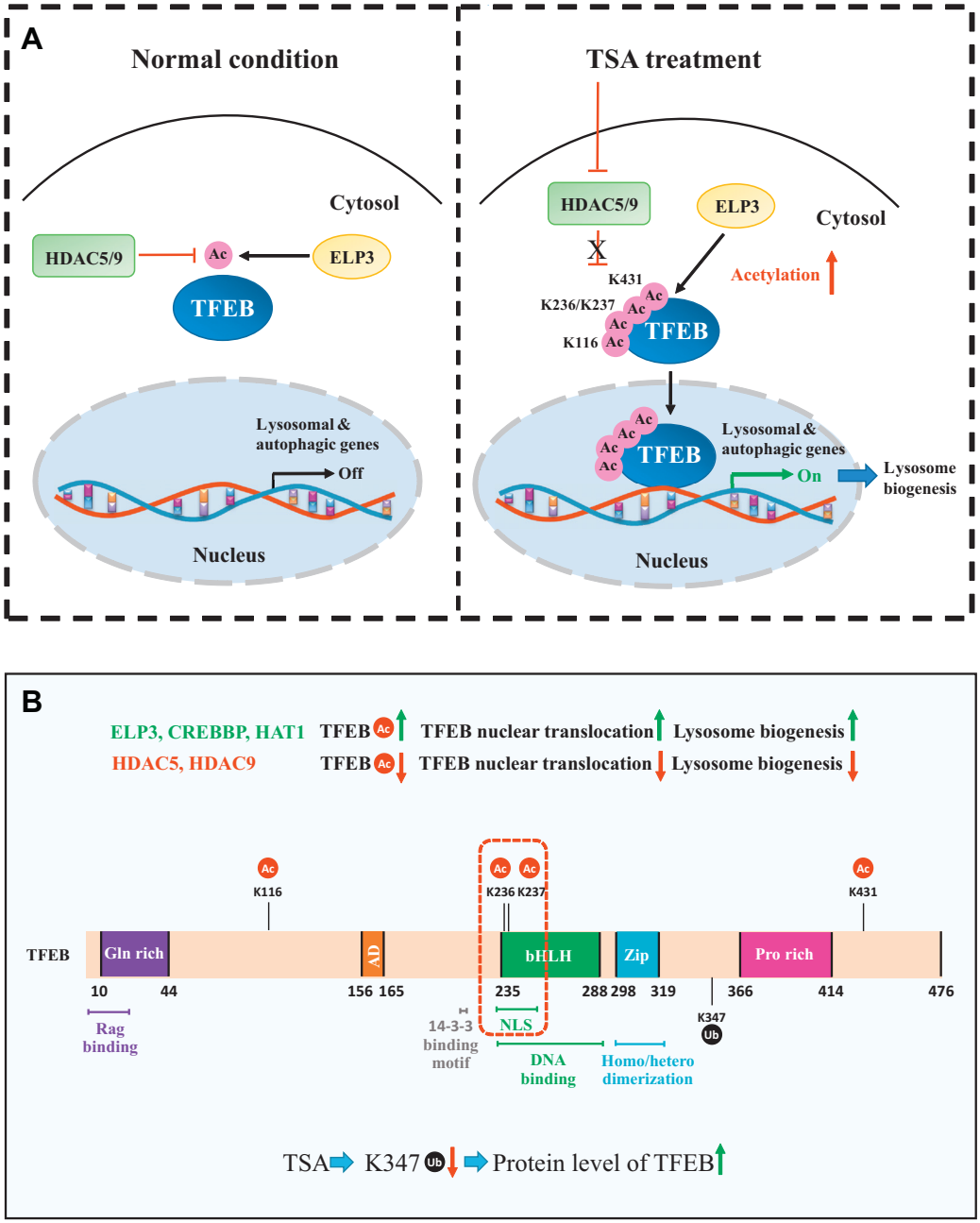

Figure 8. Regulatory mechanism of TFEB activation induced by TSA treatment. *A*, regulatory mechanism of TFEB acetylation and lysosome biogenesis induced by TSA treatment. *B*, the changes of acetylation and/or ubiquitination at indicated sites on TFEB induced by TSA treatment. TFEB, transcription factor EB; TSA, Trichostatin A.

Representative views were then selected and photographed. On the other hand, cells were cultured in DMEM containing LysoTracker Red DND-99 (0.3 μM) for 30 min. Then, the cells were suspended in PBS and transferred into tubes for quantification of LysoTracker Red staining using a CytoFLEX Flow Cytometer (Beckman). Data were analyzed using FlowJo software (FLOWJO, LLC)

Plasmids and transfection

The online tool PAIL was used to predict potential acetylation sites on human TFEB (http://bdmpail.biocuckoo.org/results.php). Human TFEB was subcloned into pEGFP-N2 plasmid. Plasmids and oligonucleotides for site-directed mutagenesis are listed in Table S3. Transient transfections were performed with Lipofectamine 2000 (Invitrogen).

mice; APP/PS1 + TSA, n = 10 mice). * indicates the comparison between the APP/PS1 + saline groups and the WT+saline group, while # indicates the comparison between the APP/PS1+TSA group and the APP/PS1+saline group. *I*,) measurement (Y maze) of the accuracy of spatial working memory in APP/PS1 mice with or without TSA injection (WT + saline, n = 15 mice; APP/PS1 + saline, n = 10 mice; APP/PS1 + TSA, n = 9 mice). For all quantifications, data (mean ± SD) were from the indicated number of independent experiments and were analyzed using *t*-tests or ANOVA. *$p < 0.05$, **$p < 0.01$, ***$p < 0.001$, $^{\#}p < 0.05$, $^{\#\#}p < 0.01$. Aβ, amyloid β; DAPI, 4′,6-diamidino-2-phenylindole; TSA, Trichostatin A.

Western blotting

After the indicated treatments, cells were harvested and lysed in ice-cold radioimmunoprecipitation assay buffer (20 mM Tris–HCl pH 7.5, 0.1% SDS, 100 mM NaCl, 0.5% sodium deoxycholate, 1 mM PMSF) containing phosphatase inhibitor cocktail (1 tablet in 10 ml) (Roche) and Complete Protease Inhibitor Cocktail (1 tablet in 50 ml). Cell lysates were cleared by centrifugation at 12,000*g* for 12 min. An equal amount of protein was resolved by SDS-PAGE and transferred onto a NC membrane. After blocking with 5% nonfat milk or bovine serum albimin, the membrane was incubated with designated primary and secondary antibodies and visualized with MiniChemi 610 chemiluminescence imager (Beijing SageCreation Science Co).

Cell fractionation

HeLa cells were treated with TSA (0.5 μM, 12 h), then nuclear and cytosolic extracts were prepared by using nuclear extraction reagents (CyNIB) and cytoplasmic extraction reagents (CIB) according to the manufacturer's instructions (Cell Signaling Technology #9038).

Quantitative real-time PCR)

mRNA was isolated from cells using TRIzol Reagent (Invitrogen). A reverse transcription reaction was performed using 1 to 2 μg of total RNA (from cells or mouse brains) with a LunaScript RT SuperMix Kit (New England BioLabs, E3010S). The mRNA levels of autophagic and lysosomal genes were determined by real-time PCR using Luna Universal qPCR Master Mix (New England BioLabs, M3003L) and qTOWER^{3}G (Analytik Jena). β-actin was used as an internal control and experiments were performed in triplicate. Primers used for qPCR in this study are listed in Table S4.

siRNAs and shRNAs

RNA oligonucleotides used for siRNA (GenePharma) and shRNA (Dharmacon, RHS4696) are listed in Table S5. For siRNA-mediated knockdown, cells were transfected with 100 pmol RNA oligonucleotides twice (at 0 h and 24 h) in 6-well plates or confocal dishes using Lipofectamine 2000. For shRNA-mediated knockdown, cells were transfected with 2 μg shRNAs for 24 h in 6-well plates or confocal dishes using DharmaFECT kb DNA transfection reagent, and then were treated with Dox (1 μM, 12 h) to induce shRNA expression (Fig. S6, *A* and *B*). The efficiency of knockdown was evaluated by quantitative real-time PCR.

In vitro *acetylation*

TFEB-His (WT or 4KR) was transformed into BL21 (DE3) and expression was induced with 0.5 mM IPTG (Amresco) at 37 °C. Bacterial cells were harvested and lysed by ultrasonication, and the proteins were analyzed by SDS-PAGE. Then, the target protein was purified by Ni-NTA beads 6FF (Bio-Rad). Flag-ELP3 protein was purified from HeLa cells 24 h after transfection by immunoprecipitation with anti-Flag affinity beads (Smart), then Flag-tagged protein was eluted with competitive elution buffer (50 mM Tris, 0.15 M NaCl, 200 μg Flag peptide (Smart)/ml, pH 7.4). For *in vitro* acetylation assay, recombinant TFEB protein was incubated with Flag-ELP3 immunoprecipitated from a cell lysate (TFEB KO cells) in the presence of acetyl-coA (1 mM) and 10 μl 5 × HAT assay buffer (250 mM Tris–HCl, pH 8.0, 5 mM DTT, 50% glycerol, 0.5 mM EDTA) in a total volume of 50 μl. The contents were gently mixed and placed in a 37 °C shaking incubator for 1 h. Then, protein loading buffer was added to the reaction and boiled for 5 min. The reaction products were subjected to SDS-PAGE and analyzed using immunoblotting.

Animals and treatment

APP/PS1 mice (strain name-B6; C3-Tg (APPswPS1dE9)/V) were purchased from Zhishan Healthcare Research Institute. These mice are double transgenic mice expressing human APP with Swedish mutations (K670N/M671L) and human PS1 gene with deletion of exon 9. All mice were maintained and bred in the animal facilities in Fudan University. APP/PS1 mice were maintained as double hemizygotes by crossing with WT mice on a C57BL/6; C3H background strain. Mice were fed with regular diets and maintained in a room at 23 °C under a 12 h (h) light–dark cycle. The APP/PS1 mice are the same mice as described previously (22). Male APP/PS1 heterozygous mice and WT littermates were used in *in vivo* experiment. Mice were randomly allocated to different groups before treatment. TSA was made at a stock concentration of 15.1 mg/ml in DMSO and then diluted to 10 mg/kg in saline. Five-month-old APP/PS1 mice (male) were given TSA (10 mg/kg) by i.p. injection every other day for 30 days, then the behavioral tests were performed and tissue samples were collected for biochemical experiments. The investigators were blinded to all animal treatments during outcome assessment. No statistical method was used to predetermine sample size and the experiments were not randomized. All procedures and husbandry were performed according to protocols approved by Fudan University.

Immunohistology

Mice were euthanized by injection of avertin after the behavioral testing, followed by *trans*-cardiac perfusion with saline and 4% paraformaldehyde. The brains were post-fixed in 4% paraformaldehyde overnight and then equilibrated in 30% sucrose. Brain sections (30 μm) were generated using a sliding microtome and stored in a −20 °C freezer as floating sections in 96-well plates filled with cryoprotectant solution (ethylene glycol, glycerol and 0.1 M phosphate buffer pH 7.4, 1:1:2 by volume). Analysis of β-amyloid immunohistology was performed on 1 out of every 12 serial floating brain sections. The primary antibody was rabbit-anti-β-amyloid (Aβ) (1:500). The secondary fluorescent antibody was donkey anti-rabbit IgG (1:500). After staining, sections were mounted, coverslipped, and maintained at 4 °C in the dark until analysis. For the quantification measurements, images were randomly

acquired throughout the hippocampus and cortex, and the Aβ-positive plaque burden was measured using NIS-Elements, BR. 3.00 software (Nikon).

For cells, the HeLa cells were fixed in 4 % paraformaldehyde and permeabilized with 0.02 % Triton X-100. Then, the cells were incubated with primary antibodies against LAMP1 (mouse monoclonal antibodies, 1:500) and further stained with Alexa Fluor 594 goat antimouse IgG antibody (1:500). 4′,6-diamidino-2-phenylindole (1:200, Beyotime) was used to visualize nuclear localization. Confocal microscopy was performed with the Confocal Laser Scanning Microscope Systems (Zeiss).

Sandwich-ELISA assay

ELISA kits for mouse Aβ42 were purchased from Invitrogen (KHB3441), and the assays were performed on lysates of mouse brains following the manufacturer's instructions.

The MWM test

The MWM test is used to measure the spatial learning ability and memory of mice (31, 32). Before the MWM test, 5-month-old APP/PS1 mice were treated with TSA (10 mg/kg) or vehicle (saline) for 1 month until the mice were 6 months old. A circular pool (diameter 120 cm, height 45 cm) was filled with water (25 °C ± 1 °C). Titanium dioxide was added to make the water opaque. The pool was divided into four equal quadrants (north, south, east, and west). A transparent platform (10 cm in diameter) was placed in the east quadrant, and its surface was 1 to 1.5 cm below the water. The mice were trained for 6 days, and each mouse performed three trials each day. The mice were released into the water at the starting position (during each trial, the mice were placed in the water at one of four starting positions; each starting position was randomly selected), and the latency to find the platform was timed. Once the platform was found, mice were allowed to sit on the platform for 10 s, and then they were dried with a towel and placed in a drying cage. If the mice were not able to find the platform within 1 min, they were gently placed on the platform for 60 s. Probe trials were performed on the seventh day. The platform was removed, and the mice were allowed to swim for 60 s. A computer-controlled video tracking system (Ethovision 11.0 (Noldus)) was used to record and analyze the behavioral data of mice.

Y maze test

The Y maze is used to assess working memory. Before the Y maze test, 5-month-old APP/PS1 mice were treated with TSA (10 mg/kg) or vehicle alone for 1 month until they were 6 months old. The Y maze was composed of three identical arms (A, B, C, 36 × 5.3 cm with 12 cm high walls), which converge at the center and are at 120° angles from each other. At the beginning, a mouse is placed at one end of an arm and allowed to move freely for 8 min. Entry into an arm was counted once all four paws entered the arm. After the behavioral experiment, mice were returned back to their cages. Finally, the apparatus was cleaned with 70% ethanol and clean paper towels before the next test. An Ethovision 11.0 video camera (Noldus) was used to record all behavioral procedures. The percent of alternation was calculated as the number of three consecutive different arm entries over the total number of entries minus two (33).

Statistics and reproducibility

Data were analyzed with Prism (GraphPad software). Statistical analyses were performed using Student's *t*-tests or ANOVA with the LSD post hoc test for normally distributed data. $^{*}p < 0.05$ was considered statistically significant. $^{**}p < 0.01$ was considered significant. $^{***}p < 0.001$ was considered extremely significant. $p > 0.05$ was considered not significant (NS).

Data availability

The mass spectrometry proteomics data have been deposited to the ProteomeXchange Consortium (http://proteomecentral.proteomexchange.org) *via* the iProX partner repository (34) with the dataset identifier PXD035879. Our data by mass spectrometry in this study are listed in Table S6.

Supporting information—This article contains supporting information.

Acknowledgments—We sincerely thank Dr Richard Youle for the TFEB KO cells. We sincerely thank Dr Dongning Pan, Yuanyuan Ruan, Yunlong Yang, Lei Lv, Yanping Xu, and Yu Zhou, for their valuable scientific suggestions. We thank Juan Qian, Xingwen Zhou, Yuanyuan Ma, Meihong Qiu, Ying Chen and Yichun Zhu for support with *in vitro* phosphorylation, mass spectrometry, flow cytometry, animal behavior tests, and confocal microscopy, respectively. We thank Dr Isabel Hanson for proofreading and editing. This work was supported by the Ministry of Science and Technology of the People's Republic of China (2022ZD0213000 to Yang Li), the National Science Foundation of China (92057103, 31872820 to Yang Li), the Innovative Research Team of High-Level Local Universities in Shanghai and a Key Laboratory Program of the Education Commission of Shanghai Municipality (ZDSYS14005 to Yang Li), the Shanghai Basic Research Program (18ZR1404000 to Yang Li), the State Key Laboratory of Drug Research (SIMM2004KF-09 to Yang Li), the National Science Foundation of China (82001550 to Jie Zhang), and China Postdoctoral Science Foundation (2020TQ0070 to Jie Zhang).

Author contributions—Y. L. conceptualization; Y. L., T. L., L. Y., X. K., and W. X. methodology; T. L. software; L. Y. and W. X. validation; J. Z. formal analysis; T. L., L. Y., X. K., and W. X. investigation; X. K., N. W., P. Y., and L. L. resources; W. X. and J. Z. data curation; T. L. and L. Y. writing–original draft; Y. L. writing–review & editing; Y. L. supervision.

Conflict of interest—The authors declare that they have no conflicts of interest with the contents of this article.

Abbreviations—The abbreviations used are: Aβ, amyloid β; AD, Alzheimer's disease; DMSO, dimethyl sulfoxide; Dox, doxycycline; HDAC, histone deacetylase; KAT, lysine acetyltransferase; LYEC,

lysosome-enhancing compound; MWM, Morris Water Maze; NLS, nuclear localization signal; TFEB, transcription factor EB; TSA, Trichostatin A.

References

1. Luzio, J. P., Pryor, P. R., and Bright, N. A. (2007) Lysosomes: fusion and function. *Nat. Rev. Mol. Cell Biol.* **8**, 622–632
2. Xu, H., and Ren, D. (2015) Lysosomal physiology. *Annu. Rev. Physiol.* **77**, 57–80
3. Settembre, C., Fraldi, A., Medina, D. L., and Ballabio, A. (2013) Signals from the lysosome: a control centre for cellular clearance and energy metabolism. *Nat. Rev. Mol. Cell Biol.* **14**, 283–296
4. Ferguson, S. M. (2015) Beyond indigestion: emerging roles for lysosome-based signaling in human disease. *Curr. Opin. Cell Biol.* **35**, 59–68
5. Efeyan, A., Comb, W. C., and Sabatini, D. M. (2015) Nutrient-sensing mechanisms and pathways. *Nature* **517**, 302–310
6. Levine, B., and Kroemer, G. (2019) Biological functions of autophagy genes: a disease perspective. *Cell* **176**, 11–42
7. Perera, R. M., and Zoncu, R. (2016) The lysosome as a regulatory hub. *Annu. Rev. Cell Dev. Biol.* **32**, 223–253
8. Bonam, S. R., Wang, F., and Muller, S. (2019) Lysosomes as a therapeutic target. *Nat. Rev. Drug Discov.* **18**, 923–948
9. Settembre, C., Di Malta, C., Polito, V. A., Garcia Arencibia, M., Vetrini, F., Erdin, S., *et al.* (2011) TFEB links autophagy to lysosomal biogenesis. *Science (New York, N.Y.)* **332**, 1429–1433
10. Sardiello, M., Palmieri, M., di Ronza, A., Medina, D. L., Valenza, M., Gennarino, V. A., *et al.* (2009) A gene network regulating lysosomal biogenesis and function. *Science (New York, N.Y.)* **325**, 473–477
11. Li, Y., Xu, M., Ding, X., Yan, C., Song, Z., Chen, L., *et al.* (2016) Protein kinase C controls lysosome biogenesis independently of mTORC1. *Nat. Cell Biol.* **18**, 1065–1077
12. Chauhan, S., Goodwin, J. G., Chauhan, S., Manyam, G., Wang, J., Kamat, A. M., *et al.* (2013) ZKSCAN3 is a master transcriptional repressor of autophagy. *Mol. Cell* **50**, 16–28
13. Settembre, C., Zoncu, R., Medina, D. L., Vetrini, F., Erdin, S., Erdin, S., *et al.* (2012) A lysosome-to-nucleus signalling mechanism senses and regulates the lysosome via mTOR and TFEB. *EMBO J.* **31**, 1095–1108
14. Martina, J. A., and Puertollano, R. (2013) Rag GTPases mediate amino acid-dependent recruitment of TFEB and MITF to lysosomes. *J. Cell Biol.* **200**, 475–491
15. Roczniak-Ferguson, A., Petit, C. S., Froehlich, F., Qian, S., Ky, J., Angarola, B., *et al.* (2012) The transcription factor TFEB links mTORC1 signaling to transcriptional control of lysosome homeostasis. *Sci. Signal.* **5**, ra42
16. Puertollano, R., and Ferguson, S. M. (2018) The complex relationship between TFEB transcription factor phosphorylation and subcellular localization. *EMBO J.* **37**
17. Yin, Q., Jian, Y., Xu, M., Huang, X., Wang, N., Liu, Z., *et al.* (2020) CDK4/6 regulate lysosome biogenesis through TFEB/TFE3. *J. Cell Biol.* **219**
18. Narita, T., Weinert, B. T., and Choudhary, C. (2019) Functions and mechanisms of non-histone protein acetylation. *Nat. Rev. Mol. Cell Biol.* **20**, 156–174
19. Bao, J., Zheng, L., Zhang, Q., Li, X., Zhang, X., Li, Z., *et al.* (2016) Deacetylation of TFEB promotes fibrillar Aβ degradation by upregulating lysosomal biogenesis in microglia. *Protein cell* **7**, 417–433
20. Zhang, J., Wang, J., Zhou, Z., Park, J. E., Wang, L., Wu, S., *et al.* (2018) Importance of TFEB acetylation in control of its transcriptional activity and lysosomal function in response to histone deacetylase inhibitors. *Autophagy* **14**, 1043–1059
21. Wang, Y., Huang, Y., Liu, J., Zhang, J., Xu, M., You, Z., *et al.* (2020) Acetyltransferase GCN5 regulates autophagy and lysosome biogenesis by targeting TFEB. *EMBO Rep.* **21**, e48335
22. Su, Q., Li, T., He, P. F., Lu, X. C., Yu, Q., Gao, Q. C., *et al.* (2021) Trichostatin A ameliorates Alzheimer's disease-related pathology and cognitive deficits by increasing albumin expression and Aβ clearance in APP/PS1 mice. *Alzheimer's Res. Ther.* **13**, 7
23. Sanna, S., Esposito, S., Masala, A., Sini, P., Nieddu, G., Galioto, M., *et al.* (2020) HDAC1 inhibition ameliorates TDP-43-induced cell death *in vitro* and *in vivo*. *Cell Death Dis.* **11**, 369
24. Guan, J. S., Haggarty, S. J., Giacometti, E., Dannenberg, J. H., Joseph, N., Gao, J., *et al.* (2009) HDAC2 negatively regulates memory formation and synaptic plasticity. *Nature* **459**, 55–60
25. Dompierre, J. P., Godin, J. D., Charrin, B. C., Cordelières, F. P., King, S. J., Humbert, S., *et al.* (2007) Histone deacetylase 6 inhibition compensates for the transport deficit in Huntington's disease by increasing tubulin acetylation. *J. Neurosci.* **27**, 3571–3583
26. Yan, S., Wei, X., Jian, W., Qin, Y., Liu, J., Zhu, S., *et al.* (2020) Pharmacological inhibition of HDAC6 attenuates NLRP3 inflammatory response and protects dopaminergic neurons in experimental models of Parkinson's disease. *Front. Aging Neurosci.* **12**, 78
27. Bento-Abreu, A., Jager, G., Swinnen, B., Rué, L., Hendrickx, S., Jones, A., *et al.* (2018) Elongator subunit 3 (ELP3) modifies ALS through tRNA modification. *Hum. Mol. Genet.* **27**, 1276–1289
28. Simpson, C. L., Lemmens, R., Miskiewicz, K., Broom, W. J., Hansen, V. K., van Vught, P. W., *et al.* (2009) Variants of the elongator protein 3 (ELP3) gene are associated with motor neuron degeneration. *Hum. Mol. Genet.* **18**, 472–481
29. Rouaux, C., Jokic, N., Mbebi, C., Boutillier, S., Loeffler, J. P., and Boutillier, A. L. (2003) Critical loss of CBP/p300 histone acetylase activity by caspase-6 during neurodegeneration. *EMBO J.* **22**, 6537–6549
30. Jeong, H., Then, F., Melia, T. J., Jr., Mazzulli, J. R., Cui, L., Savas, J. N., *et al.* (2009) Acetylation targets mutant huntingtin to autophagosomes for degradation. *Cell* **137**, 60–72
31. Morris, R. (1984) Developments of a water-maze procedure for studying spatial learning in the rat. *J. Neurosci. Met.* **11**, 47–60
32. Nagakura, A., Shitaka, Y., Yarimizu, J., and Matsuoka, N. (2013) Characterization of cognitive deficits in a transgenic mouse model of Alzheimer's disease and effects of donepezil and memantine. *Eur. J. Pharmacol.* **703**, 53–61
33. Yeshurun, S., Rogers, J., Short, A. K., Renoir, T., Pang, T. Y., and Hannan, A. J. (2017) Elevated paternal glucocorticoid exposure modifies memory retention in female offspring. *Psychoneuroendocrinology* **83**, 9–18
34. Ma, J., Chen, T., Wu, S., Yang, C., Bai, M., Shu, K., *et al.* (2019) iProX: an integrated proteome resource. *Nucl. Acids Res.* **47**, D1211–d1217